Two dimensional Leidenfrost droplets in a Hele-Shaw cell

Franck Celestini, Thomas Frisch, Alexandre Cohen, Christophe Raufaste, Laurent Duchemin, and Yves Pomeau

Citation: Physics of Fluids (1994-present) **26**, 032103 (2014); doi: 10.1063/1.4867163
View online: http://dx.doi.org/10.1063/1.4867163
View Table of Contents: http://scitation.aip.org/content/aip/journal/pof2/26/3?ver=pdfcov
Published by the AIP Publishing

PHYSICS OF FLUIDS **26**, 032103 (2014)

Two dimensional Leidenfrost droplets in a Hele-Shaw cell

Franck Celestini,[1] Thomas Frisch,[2,a)] Alexandre Cohen,[1]
Christophe Raufaste,[1] Laurent Duchemin,[3] and Yves Pomeau[4]
[1]*Université de Nice Sophia-Antipolis, CNRS, LPMC, UMR 7336, Parc Valrose, 06108 Nice Cedex 2, France*
[2]*Université de Nice Sophia-Antipolis, CNRS, INLN, UMR 7335, 1361 Routes des lucioles, Sophia Antipolis, F-06560 Valbonne, France*
[3]*Institut de Recherche sur les phénomènes hors-équilibre, CNRS UMR 7342, Aix-Marseille Université, 49 rue Joliot Curie, 13384 Marseille, France*
[4]*Department of Mathematics, University of Arizona, Tucson, Arizona 85721, USA*

(Received 4 November 2013; accepted 7 February 2014; published online 5 March 2014)

We experimentally and theoretically investigate the behavior of Leidenfrost droplets inserted in a Hele-Shaw cell. As a result of the confinement from the two surfaces, the droplet has the shape of a flattened disc and is thermally isolated from the surface by the two evaporating vapor layers. An analysis of the evaporation rate using simple scaling arguments is in agreement with the experimental results. Using the lubrication approximation we numerically determine the shape of the droplets as a function of its radius. We furthermore find that the droplet width tends to zero at its center when the radius reaches a critical value. This prediction is corroborated experimentally by the direct observation of the sudden transition from a flattened disc into an expending torus. Below this critical size, the droplets are also displaying capillary azimuthal oscillating modes reminiscent of a hydrodynamic instability. © *2014 AIP Publishing LLC*. [http://dx.doi.org/10.1063/1.4867163]

I. INTRODUCTION

In spite of its discovery in the late 19th century,[1] the Leidenfrost phenomenon is still today the subject of numerous studies for two essential reasons. The first reason is related to the strong decrease of the thermal exchange between the solid and the liquid due to the presence of low thermal conductivity vapor layers: this situation is of importance, for example, in metallurgy to control the cooling of metals[2] or in nuclear reactor safety.[3] The second is fundamental and related to the fact that a Leidenfrost droplet may be considered as an ideal realization of a perfect non-wetting system. These droplets have shown rich and unexpected behaviors.[4–6] For example, drops on periodic patterned surface display a drift due to the spatial symmetry breaking. Furthermore, possible applications of Leidenfrost droplets might be the transport of liquid in the milli-fluidic or micro-fluidic area.[7] For example, low pressure Leidenfrost droplets have been shown recently to be stable at room temperature and could be subsequently potential receptor of particles in solution.[8] Surprisingly, to our knowledge no studies have been devoted yet to the Leidenfrost effect in a 2D confined geometry. This is somehow unexpected because such a complex phenomenon should display new properties as the spatial dimension is reduced. The aim of this paper is thus to investigate a simple situation representative of the effect of spatial confinement on the Leidenfrost droplets. These droplets are inserted in a horizontal Hele-Shaw cell whose gap is smaller than the capillary length $\kappa^{-1} = \sqrt{\gamma/\rho_l g}$ with γ being the surface tension, ρ_l the liquid density, and g the acceleration of gravity. As a result of the confinement from the two surfaces the drop takes the shape of a flattened saucer-like disc which floats between two vapor layers. These drops are quasi thermally isolated from the surface by the evaporating vapor layers and they display undulating star-like shapes. In this article, we first

a)Electronic mail: thomas.frisch@unice.fr

describe our experimental set-up and we describe the dynamic of evaporation by a simple model which takes into account the Poiseuille flow in the vapor layer. This model is in agreement with the experimental results for the global evaporation rates. We then discuss the vertical profile of the drop using a theoretical model which results from the balance between surface tension and the Poiseuille flow in the vapor layer. We observed that the droplets have a maximum radius R_c beyond which they transform into a torus by the process of a hole nucleation and expansion at their center. These experimental results are confronted with our theoretical model and fall within a good agreement. We also report observations of large amplitude star-like undulation consisting of azimuthal oscillating capillary wave. The frequency of oscillations is measured and is found to be close to the frequency of Rayleigh capillary wave of droplets. Finally, we discuss possible mechanisms at the origin of the instability leading to star-like oscillations of the droplets.

II. EVAPORATION DYNAMIC

A. Experimental results

Our experimental set-up is depicted in Fig. 1. A heated copper block permits to control the temperature T_p of two plates separated by a spacing of width d. This temperature is measured with a PT100 temperature sensor. The upper plate is made of sapphire whose optical and thermal properties permit us to visualize the droplet from the top through a semi-transparency mirror. The lower plate is covered with a silicon wafer. Images are recorded with a high speed camera with a frame rate varying between 60 and 4000 frames per second. As for classical Leidenfrost droplets we suppose that the liquid is at its boiling temperature T_b and we denote $\Delta T = T_p - T_b$ the temperature difference between the hot plates and the droplet. For all the experiments, the plate temperature has been fixed to $T_p = 300\,^{\circ}\mathrm{C}$, giving a value of $\Delta T = 200\,^{\circ}\mathrm{C}$. A capillary is used to insert the ultra distilled water droplet into the Hele-Shaw cell. Different spacings d have been used ranging between $d = 0.3$ and 2 mm.

We first investigate the dynamics of the evaporating droplets. The lifetime of the droplet is about 10 s, one order of magnitude lower than usual Leidenfrost droplets and two orders of magnitude lower than low pressure Leidenfrost droplets.[8] Qualitatively, the decrease of the life time of the droplet compared to the usual Leidenfrost droplets at ambient pressure is due to the fact that the droplet is heated on both sides and confined so that its contact area with the confining heated plates is larger. As illustrated in Fig. 2, the droplet is slowly evaporating and its radius R is decreasing with time. An image analysis permits to record the evolution of R with the time t, its value is deducted from the apparent area of the droplet viewed from the top. It is worth noticing that the shape of the drop is not necessary circular but presents some contour oscillations that will be discussed in Sec. IV

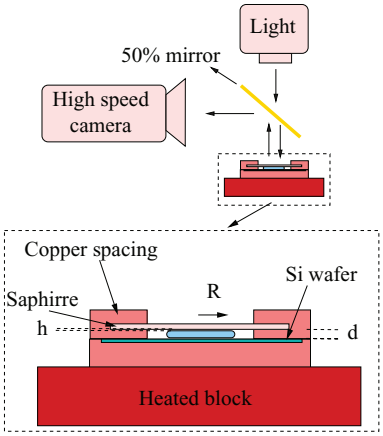

FIG. 1. Experimental set-up: a Hele-Shaw cell is heated at a controlled temperature T_P. A Leidenfrost droplet of radius R is inserted between the two hot plates separated by a spacing d.

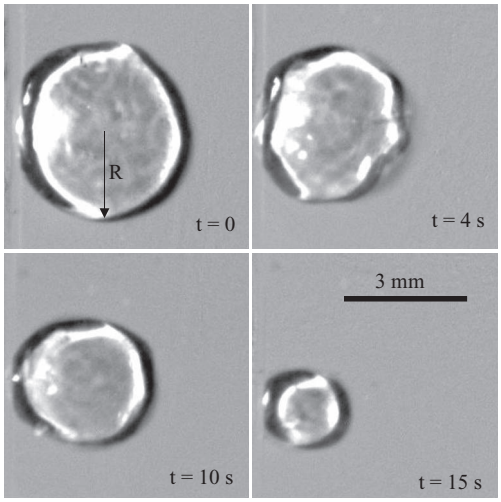

FIG. 2. Snapshots of an evaporating droplet (top view) at different times. The spacing of the Hele-Shaw cell is of 1 mm and the temperature of the plates is $T_p = 300\,^{\circ}\mathrm{C}$.

of this article. We represent in Fig. 3 the time evolution of the radius R for droplets inserted in three cells with different spacings: $d = 0.3$, 0.5, and 1 mm. We clearly see that the lower the spacing the faster the evaporation of the droplet. The full lines correspond to a best-fit of the phenomenological model which is presented just below.

B. Phenomenological model

One of the difficulties in the Leidenfrost system consists in the determination of the thickness h of the vapor film which is situated between the drop and the heated plates. In order to estimate h we develop a model based on a simple scaling argument which applies to a flat droplet of radius R as shown on Fig. 1. The vapor film thickness results from the balance between the pressure (driven by the Poiseuille flow produced by the local vapor evaporation) and the capillary surface tension effects. Energy conservation during the evaporation process (namely, Stefan's boundary condition on the liquid-vapor interface) and Fourier law for the heat transfer in the film yield the order of magnitude for the vertical velocity w of the vapor near the surface of the droplet. It reads

$$\rho_v L w \propto \lambda \Delta T / h\,. \tag{1}$$

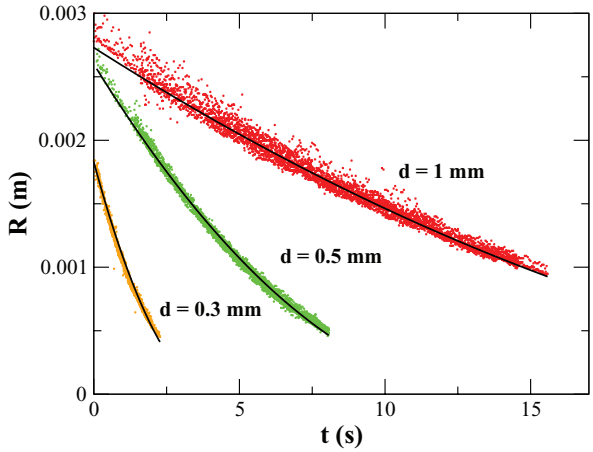

FIG. 3. Droplet radius as a function of time for three different spacings $d = 1$, 0.5, and 0.3 mm, respectively, in mid-gray, lighter gray, and darker gray circles (red, green, and brown, respectively). The full lines correspond to the best fit to Eq. (9).

Here, L is the latent heat per unit mass, λ is the thermal diffusivity coefficient, ΔT is the temperature difference between the hot plates and the droplet, and ρ_v is the density of the vapor. Mass conservation yields the following estimate for the magnitude of the horizontal velocity u in terms of the vertical velocity w:

$$u/R \propto w/h\,. \tag{2}$$

Assuming a Poiseuille flow in the vapor in the lubrication regime leads to a horizontal pressure drop ΔP which scales as

$$\Delta P/R \propto \eta u/h^2\,, \tag{3}$$

where η is the vapor film viscosity.

Finally, we note that the Laplace pressure ΔP between the drop and the gas reads

$$\Delta P \propto \gamma/d\,. \tag{4}$$

Here, we have neglected the small curvature term which is smaller by a factor d/R.

We obtain using Eqs. (1)–(4) a relation for the film height h which reads

$$h \propto R^{1/2} d^{1/4} \left(\frac{\eta\lambda\Delta T}{\rho_v L\gamma}\right)^{1/4}\,, \tag{5}$$

which can be rewritten simply as

$$h \propto R^{1/2} d^{1/4} l^{1/4}\,, \tag{6}$$

where we have introduced a characteristic length l defined as

$$l = \frac{\eta\lambda\Delta T}{\rho_v L\gamma}\,. \tag{7}$$

As shown by Eq. (6), the width of the vapor layer h can thus be deduced from the measured value R.

Furthermore, we can also verify experimentally that the previous scaling holds by measuring the time evolution of the radius of the drop $R(t)$. The rate of evaporation of the droplet can be deduced from the outgoing flux of vapor and reads

$$\rho_l \frac{d}{dt}(\pi R^2 d) \propto 2\rho_v \pi R^2 w\,. \tag{8}$$

Solving these differential equations using Eqs. (1) and (6) we obtain the evolution radius $R(t)$ as

$$R(t) \propto (R_0^{1/2} - Ct)^2\,. \tag{9}$$

Here

$$C = \frac{\lambda\Delta T}{\rho_l L l^{1/4}} d^{-5/4}\,. \tag{10}$$

As shown on Fig. 3, we compare the experimental measurements of the time evolution of the radius $R(t)$ with the theoretical prediction given in Eq. (9) for three different values of the spacing d. A satisfactory agreement is found between the theory and the experiments. We can infer the value of the constant C from a best-fit adjustment of the data given in Fig. 3 using the time evolution for $R(t)$ given in Eq. (9). As shown in Fig. 4 the values of C obtained lead to the expected dependence $C \propto d^{-5/4}$ as predicted by Eq. (10). It is worth noticing that the value of the pre-factor $\lambda\Delta T/(\rho_l L l^{1/4})$ found experimentally using the data shown in Fig. 3 is $2.9 \times 10^{-7}\,\mathrm{m}^{1/2}\,\mathrm{s}^{-1}$. It is of same order than the one predicted $5.4 \times 10^{-7}\,\mathrm{m}^{1/2}\,\mathrm{s}^{-1}$.

Here, we have used the following values for the physical parameters: $\lambda = 0.032\,\mathrm{J\,s^{-1}K^{-1}}$, $L = 2.25 \times 10^6\,\mathrm{J\,kg^{-1}}$, $\rho_v = 0.81\,\mathrm{kg\,m^{-3}}$, $\eta = 1.3 \times 10^{-5}\,\mathrm{kg\,m^{-1}\,s^{-1}}$, $\kappa = \lambda/(L\rho_v)$, $\Delta T = 200\,^\circ\mathrm{C}$, $\sigma = 0.072\,\mathrm{Jm^{-2}}$ and $d = 0.001$ m.

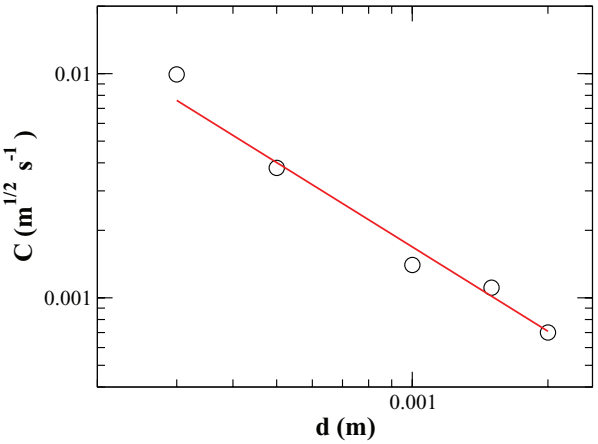

FIG. 4. Values of the parameter C as a function of the spacing d. The full line corresponds to the scaling law predicted in Eq. (10).

III. DROPLET SHAPE AND HOLE NUCLEATION

The previous analysis is based upon a strong hypothesis of a constant vapor thickness, both below and above the droplet. It has been recently shown that this hypothesis does not hold properly for 3D Leidenfrost droplet.[6,9] Therefore, we decided to perform a deeper theoretical analysis to predict the vapor layer profile in our confined geometry.

A. Lubrication model

Let the height of the vapor layer at the equator be h_0, the neck height h_n and the radius of the droplet be R as shown in Fig. 5. The two plates are held at temperature T_p and are separated by a distance d, the temperature of the drop is T_b. Let $h(r)$ be the shape on the lower interface and $d - h(r)$ the shape of the upper interface. The balance between the surface tension effect and the Poiseuille flow leads to a variety of shapes which can be described using the lubrication approximation. This approach has been used successfully in another context such as lens floating.[10] The pressure p in the vapor film just outside the drop is driven by the following equation as shown in the Appendix and in Ref. 9:

$$\partial_r \left(\frac{r h^3}{12} \partial_r p \right) + \frac{r \eta \kappa \Delta T}{h(r)} = 0 \,, \tag{11}$$

where $\kappa = \lambda/(\rho_v L)$. Equation (11) derives from the incompressibility condition of the vapor and the Poiseuille hydrodynamic relation.[9] The pressure in the vapor film just below the drop is given by

$$p = p_d - \sigma \kappa \,. \tag{12}$$

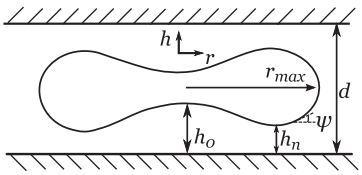

FIG. 5. Sketch of a vertical cut of a drop. h_0, h_n, R and the angle ψ are shown. Here, ψ is the angle between the tangent to the surface of the drop and the horizontal axis r.

Here, p_d is the pressure in the drop which is supposed to be constant, σ is the surface tension, and κ is the mean curvature which reads

$$\kappa = \partial_s \psi + \sin\psi / r \,, \tag{13}$$

here the angle ψ represents the tangent angle to the surface of the drop with respect to the horizontal r axis as shown in Fig. 5. Let us choose d as the unit of length and σ/d the pressure unit. In these units Eq. (11) reads

$$\partial_r \left(\frac{r h^3}{12} \partial_r p \right) + \frac{r\alpha}{h} = 0 \,, \tag{14}$$

where $\alpha = \frac{\eta \kappa \delta T}{\sigma d}$ is a dimensionless parameter which depends on d.

The lubrication Eqs. (13) and (14) can be reformulated similar to Ref. 10 using the arc length s along the drop as

$$\partial_s h = \sin\psi \,, \tag{15}$$

$$\partial_s r = \cos\psi \,, \tag{16}$$

$$\partial_s \psi = \kappa - \sin\psi / r \,, \tag{17}$$

$$\partial_s \kappa = \kappa_1 \,, \tag{18}$$

$$\partial_s \kappa_1 = \frac{12\alpha \cos^2(\psi)}{h^4} - \frac{3\kappa_1 h'}{h} - \frac{\kappa_1 (r\psi' \tan(\psi) + r')}{r} \,. \tag{19}$$

Here, we have used the following geometric transformation $\partial_r = \partial_s \frac{\partial s}{\partial r} = \frac{\partial_s}{\cos(\psi)}$. The boundary conditions at $r = 0$ which is located on the symmetry axis read

$$r(s = 0) = 0 \,, \tag{20}$$

$$h(s = 0) = h_0 \,, \tag{21}$$

$$\psi(0) = 0 \,, \tag{22}$$

$$\kappa(0) = \kappa_0 \,, \tag{23}$$

$$\partial_s \kappa(0) = 0 \,. \tag{24}$$

The boundary conditions at $s = s_{max}$ which corresponds to the equator read

$$r(s = s_{max}) = R \,, \tag{25}$$

$$h(s_{max}) = 1/2 \tag{26}$$

$$\psi(s_{max}) = \pi/2 \tag{27}$$

$$\partial_s \kappa(s_{max}) = 0. \tag{28}$$

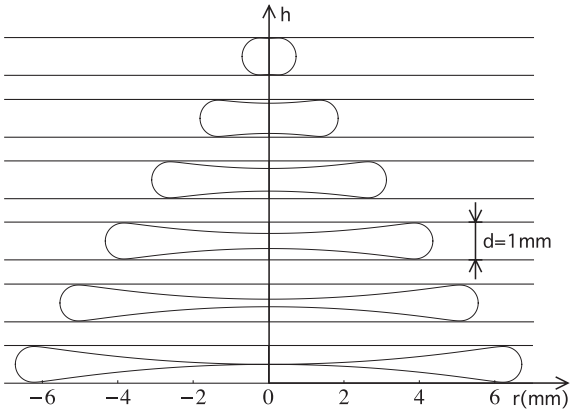

FIG. 6. Profile of a drop obtained by numerical resolutions of Eqs. (15)–(19) for 6 different values of the parameters h_0. Top $h_0 = 0.001$ mm, bottom $h_0 = 0.5$ mm. The horizontal axis is r, the vertical axis is the z axis. The vertical distance d between the two plates is 1 mm. The bottom curve represents the curve for which $R = R_c$.

There are two free parameters κ_o and s_{max} which need to be adjusted in order to satisfy the boundary conditions defined in Eqs. (27) and (28). These equations can be solved using a standard shooting method. As shown in Fig. 6, we represent the shape of the drop for different values of the h_0, we find that there exists a critical radius R_c beyond which a simply connected drop cannot exist as shown, for example, on the bottom profile displayed in Fig. 6. Even though the direct measurement of vertical profile of the droplet is not possible, we have estimated the value of the vapor layer h by proceeding in the following manner. Using the relation obtained in Eq. (5) we can estimate the value of h by a measurement of R. Here, the value for the pre-factor in Eq. (5) is deducted from the experimental measurement of the constant C, the pre-factor in Eq. (10) is estimated using a best-fit adjustment of the results shown in Fig. 3. Finally, we display in Fig. 7 the value of h_0 and h_n obtained by numerical simulation of Eqs. (15)–(19) as a function of R for two values of the spacing d. We superpose on these curves the value of the thickness h estimated above. As expected the value of h ranges between h_{neck} and h_0.

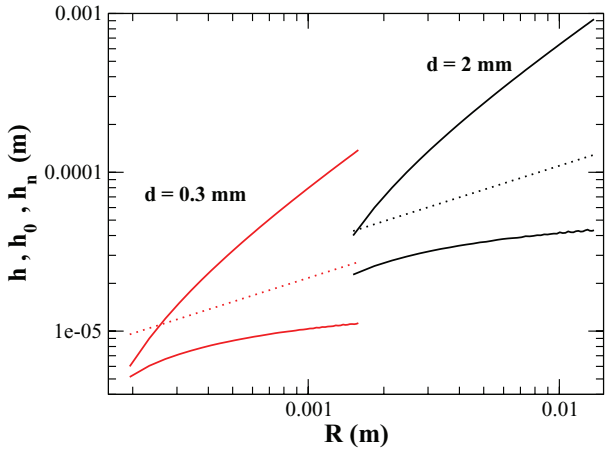

FIG. 7. Numerical simulation of Eqs. (15)–(19). We plot h_0 and h_n (full lines, respectively, top and bottom) as a function of R. The red curve is for $d = 0.3$ mm, the black is for $d = 2$ mm. The dashed-lines represent the scaling $h \propto R^{1/2}$ predicted by Eq. (5) using the data deduced from the experimental measurement of the constant C. The prefactor in Eq. (10) is estimated using a best-fit adjustment of the results shown in Fig. 3.

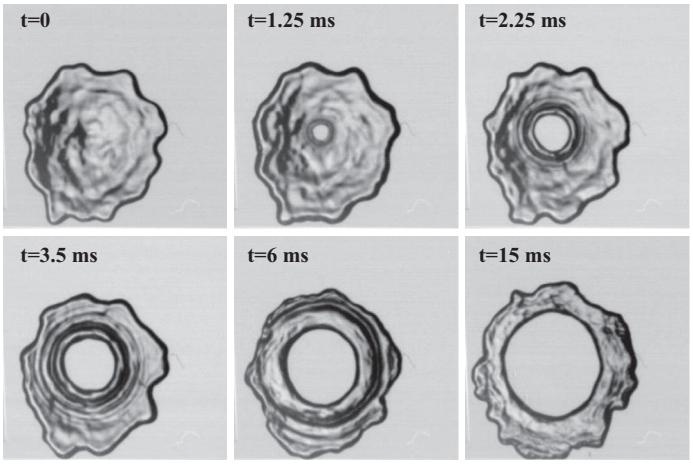

FIG. 8. Critical radius R_c versus the spacing d. Each point corresponds to one experiment. The solid line (red) holds for the numerical prediction using Eqs. (15)–(19).

B. Hole nucleation

The numerical resolution of the droplet profile as shown in Sec. III A reveals that no solution should exist beyond a critical drop radius R_c. This statement is thus tested experimentally: we first inject a primary drop in our system that is grown continuously by coalescence with smaller drops. We find that at some point a hole nucleates and grows inside the drops (Fig. 8). The hole grows until the expanding torus reaches the edges of our experimental set-up. The critical radius R_c exhibits some dispersion, but a clear trend can be observed as a function of the spacing d (Fig. 9). The comparison with the model is rather satisfactory given that there is no free parameter. The agreement is even very good for smaller spacing. For larger spacing we might expect some discrepancies since gravitational effects could play a role as the spacing becomes comparable to the capillary length $l_c = \sqrt{\sigma/\rho g}$.

IV. OSCILLATION MODES

In our experiment, the drops were found to have radial oscillations mode for most of the values of the parameters such as the radius R and the spacing between the two plates d. Theses oscillations can be described by star-shaped contour modes with frequencies ranging between 10 and 400 Hz.

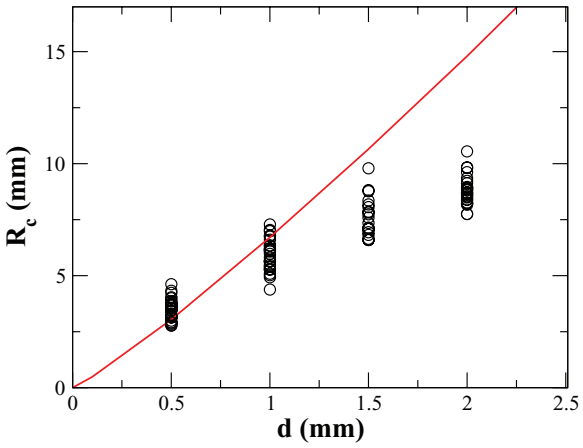

FIG. 9. Image sequences of the hole nucleation and growth.

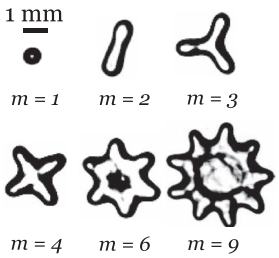

FIG. 10. Top views of the droplets. Examples of different oscillation modes. Here, m holds for the number of spikes of the drop, $d = 1$ mm and the horizontal scale is shown by the black bar.

The modes are thus parametrized by an integer m, namely, the azimuthal mode number, which measures the number of spikes along the contour of the drop as shown in Fig. 10. In Fig. 11, we display the evolution of the droplet for the $m = 3$ mode during a half-period, this oscillation is typical of a standing wave pattern.

During a typical experiment in which drops slowly evaporate, we observe that the azimuthal number m has a tendency to decrease with time as the drop size decreases. However, there seems to be no stringent dynamics for the time evolution of the azimuthal mode number and in particular a wide range of frequency transitions occurs during the life of a droplet. Furthermore, there seems to be no direct link between the azimuthal number m and the droplet radius except for this decreasing tendency. The value of the mode number displays strong stochasticity probably induced by the nonlinear coupling between oscillation modes and by the inherent thermal fluctuations which are expected at liquid-vapor interfaces just below the boiling transition.

We plot in Fig. 12 the frequency measurements with respect to the radius R for different values of m. They reveal a clear trend well approximated by a power law as explained below. Let us first focus, for example, on the mode $m = 3$ which was observed over the larger range of frequencies and for several values of the spacing d. We did not notice any effect of the spacing so that we performed a power law interpolation over all its data. This leads to $f(\text{Hz}) = (12 \pm 1) \times 10^{-4} R(\text{mm})^{-1.7 \pm 0.3}$. Even though other modes m do not span as much frequencies as the mode $m = 3$ does, their trends are also compatible with a scaling of $R^{-3/2}$. Such an exponent is therefore reminiscent of the Rayleigh spectrum for capillary wave on spherical drops[11,12] or two dimensional discs[13] for which the frequency also scales like $R^{-3/2}$. In order to go deeper in this analysis we have plotted in Fig. 13 the dimensionless frequency f/f_0 of the contour modes as a function of m, where $f_0 = \frac{1}{2\pi}\sqrt{\frac{\gamma}{\rho R^3}}$ is the typical frequency scale. The comparisons between the experimental points and the theoretical results shown in Fig. 13 seem to validate the capillary origin of these surface waves. The small discrepancy emphasized by the slight overestimate of the theory may origin from several facts such as the complexity of the Leidenfrost effect which involves vapor flow around the droplet, the possible

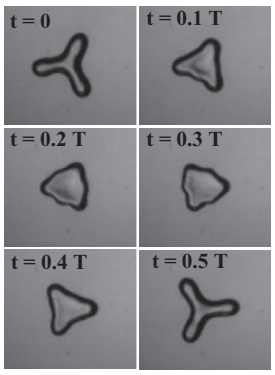

FIG. 11. Top view of a single droplet. Time evolution of the $m = 3$ mode for a half-period. Here $d = 1$ mm, $R = 1$ mm, and $\mathbf{T} = 0.009$ s.

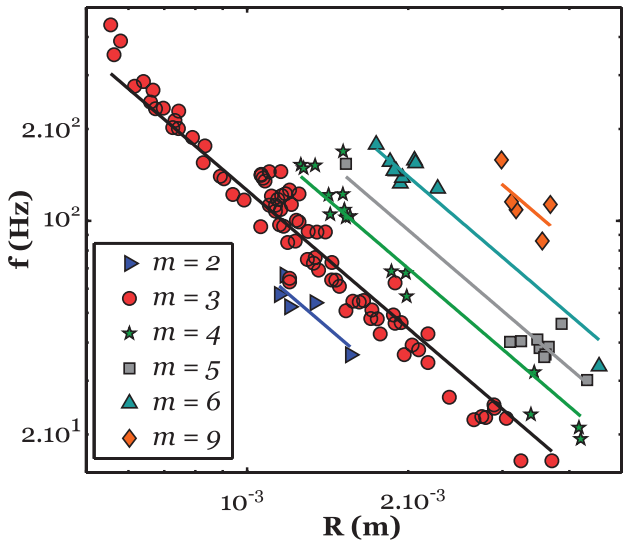

FIG. 12. Oscillation frequency f versus the drop radius R in meters. Several modes are represented. Each of them is fitted by a power law with an exponent $-3/2$ (solid lines). Experiments are performed for $d = 1$ mm, excepted for $m = 3$, where data of $d = 0.5$ and 0.3 mm are also plotted.

coupling between the gas dynamics and the fluids at the surface and the particular geometry of a droplet in a Hele-Shaw cell.

It is worth comparing our experimental results with the non-confined 3D droplet systems. Star-like drop shapes can be observed when a liquid nitrogen droplet is deposited on a solid substrate[14] or on a liquid bath.[15] Spontaneous oscillation of drop or liquid puddles seems to be more general and has also been observed in other levitated systems without Leidenfrost effect as shown in Ref. 16. In this article, a liquid droplet or puddle is levitated over an air cushion which generates a quasi-laminar flow and star-like oscillations are observed.[16] In all these systems, Leidenfrost and levitated air-cushion drops, the relevant frequency of oscillations displays a $R^{-3/2}$ tendency which is a characteristic of Rayleigh capillary wave dispersion relation.[15,17]

While shape oscillations are encountered in many systems without need of any oscillating forcing, the origin of this instability remains unravel and is still a matter of debate as discussed

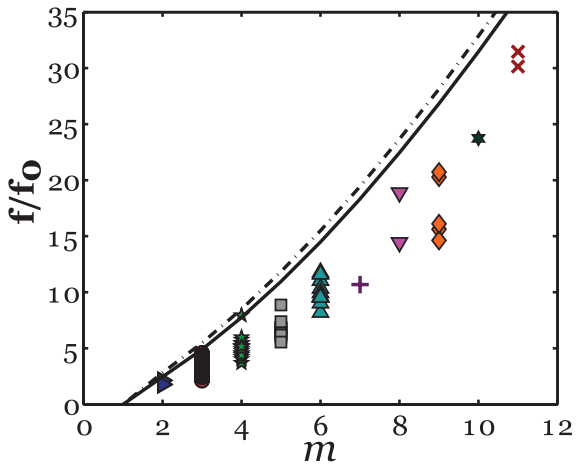

FIG. 13. Dimensionless oscillation frequency f/f_0 vs the mode number m. All experiments are plotted ($d = 0.3$, 0.5, 1, and 2 mm). For comparison we plot the models of an inviscid 3D spherical drop of the same radius[11,12] ($f^{3D}/f_0 = \sqrt{(m-1)m(m+2)}$, dashed-dotted line) and for a perfectly homogeneous and discoidal 2D puddle[13] ($f^{2D}/f_0 = \sqrt{m(m^2-1)}$, solid line).

in Ref. 16. In the case of air flow levitated droplet, it was observed that an instability leading to star-like shapes appears above a critical air flow rate. It was proposed[17] that an axisymmetric mode appears due to an unstable hydrodynamics flow in the lubrication layer. This primary instability may trigger parametrically the appearance of a non axisymmetric contour mode. This parametric coupling between the axisymmetric mode and the contour mode has already been reported for sessile droplets undergoing external periodic forcing.[18] This could support the hypothesis of a purely hydrodynamical instability in our experiments as well.

V. CONCLUSION

We have investigated the behavior of 2D-Leidenfrost droplet in a Hele-Shaw cell. This investigation has revealed a rich behavior of phenomena such as droplet levitation below and above a vapor layer, and the appearance of critical transition from discoidal droplet to torus like droplet. This topological transition occurs due to the thinning of liquid at the center of the droplet. We have characterized experimentally these phenomena and we have presented a theoretical model and a numerical study based on the lubrication approximation which corroborate these experimental facts. We are currently investigating the dynamics of the hole expansion. We also report observations of large amplitude star-like undulation consisting of azimuthal oscillating capillary waves. The frequency of oscillations is measured and is found to be close to the frequency of Rayleigh capillary wave of droplets. Finally, we have discussed possible mechanisms which are at the origin of this instability.

ACKNOWLEDGMENTS

We would like to thank Martine Le Berre, Christophe Josserand, Damien Scandola, and Philippe Brunet for fruitful discussions and the federation Wolfgang Doeblin CNRS for financial support.

APPENDIX: DERIVATION OF THE LUBRICATION MODEL

For the sake of clarity, we derive here Eq. (11). Let us recall that the temperature in the vapor layer is given by

$$T = T_p\left(1 - \frac{z}{h(x,\,y)}\right) + T_b\frac{z}{h(x,\,y)}\,. \tag{A1}$$

The horizontal velocity components u and v read using the lubrication approach:

$$u = \frac{z(z-h(x,\,y))}{2\eta}\partial_x p \;\text{ and }\; v = \frac{z(z-h(x,\,y))}{2\eta}\partial_y p\,.$$

Integrating the incompressibility relation,

$$\partial_x u + \partial_y v + \partial_z w = 0\,,$$

between $z = 0$ where $w = 0$ and $z = h(x, y)$ we obtain using Eq. (1),

$$\nabla_2 \cdot \left(\frac{h^3}{12}\nabla_2 p\right) + \frac{\eta\kappa\,\Delta T}{h(x,\,y)} = 0\,, \tag{A2}$$

where $\kappa = \lambda/(\rho_v L)$ and $\nabla_2 = \mathbf{e}_x\partial_x + \mathbf{e}_y\partial_y$. In cylindrical coordinates, Eq. (A2) reads

$$\partial_r\left(\frac{rh^3}{12}\partial_r p\right) + \frac{r\eta\kappa\,\Delta T}{h(r)} = 0 \tag{A3}$$

and is exactly similar to Eq. (11).

[1] J. G. Leidenfrost, *De Aquae Communis Nonnullis Qualitatibus Tractatus* (Ovenius, Duisbourg, 1756).
[2] J. D. Bernardin and I. Mudawar, "The Leidenfrost point: Experimental study and assessment of existing models," J. Heat Transfer **121**, 894 (1999).
[3] H. van Dam, "Physics of nuclear reactor safety," Rep. Prog. Phys. **55**, 2025 (1992).

[4] D. Quéré, "Leidenfrost dynamics," Annu. Rev. Fluid. Mech. **45**, 197 (2013).
[5] A.-L. Biance, C. Clanet, and D. Quéré, "Leidenfrost drops," Phys. Fluids **15**, 1632 (2003).
[6] F. Celestini, T. Frisch, and Y. Pomeau, "Take-off of small Leidenfrost droplets," Phys. Rev. Lett. **109**, 034501 (2012).
[7] P. Tabeling, *Introduction to Microfluidics* (Oxford University Press, Oxford, 2005).
[8] F. Celestini, T. Frisch, and Y. Pomeau, "Room temperature water Leidenfrost droplets," Soft Matter **9**, 9535 (2013).
[9] Y. Pomeau, M. Le Berre, F. Celestini, and T. Frisch, "The Leidenfrost effect: From quasi-spherical droplets to puddles," C. R. Mec. **340**, 867 (2012).
[10] L. Duchemin, J. Lister, and U. Lange, "Static shapes of a viscous levitated drop," J. Fluid Mech. **533**, 161–170 (2005).
[11] H. Lamb, *Hydrodynamics*, 6th ed. (Cambridge University Press, Cambridge, USA, 1932).
[12] L. Rayleigh, "On the capillary phenomena of jets," Proc. R. Soc. London **29**, 71–97 (1879).
[13] R. Takaki and K. Adachi, "Vibration of a flattened drop. II. Normal mode analysis," J. Phys. Soc. Jpn. **54**, 2462–2469 (1985).
[14] D. E. Strier, A. A. Duarte, H. Ferrari, and G. B. Mindlin, "Nitrogen stars: morphogenesis of a liquid drop," Physica A **283**, 261 (2000).
[15] A. Snezhko, E. Ben Jacob, and I. S. Aranson, "Pulsating gliding-transition in the dynamics of levitating liquid nitrogen droplets," New J. Phys. **10**, 043034 (2008).
[16] P. Brunet and J. H. Snoeijer, "Star-drops formed by periodic excitation and on an air cushion: A short review," Eur. Phys. J.: Spec. Top. **192**, 207–226 (2011).
[17] W. Bouwhuis, K. G. Winkels, I. R. Peters, P. Brunet, D. van der Meer, and J. H. Snoeijer, "Oscillating and star-shaped drops levitated by an airflow," Phys. Rev. E **88**, 023017 (2013).
[18] X. Noblin, A. Buguin, and F. Brochard-Wyart, "Triplon modes of puddles," Phys. Rev. Lett. **94**, 166102 (2005).